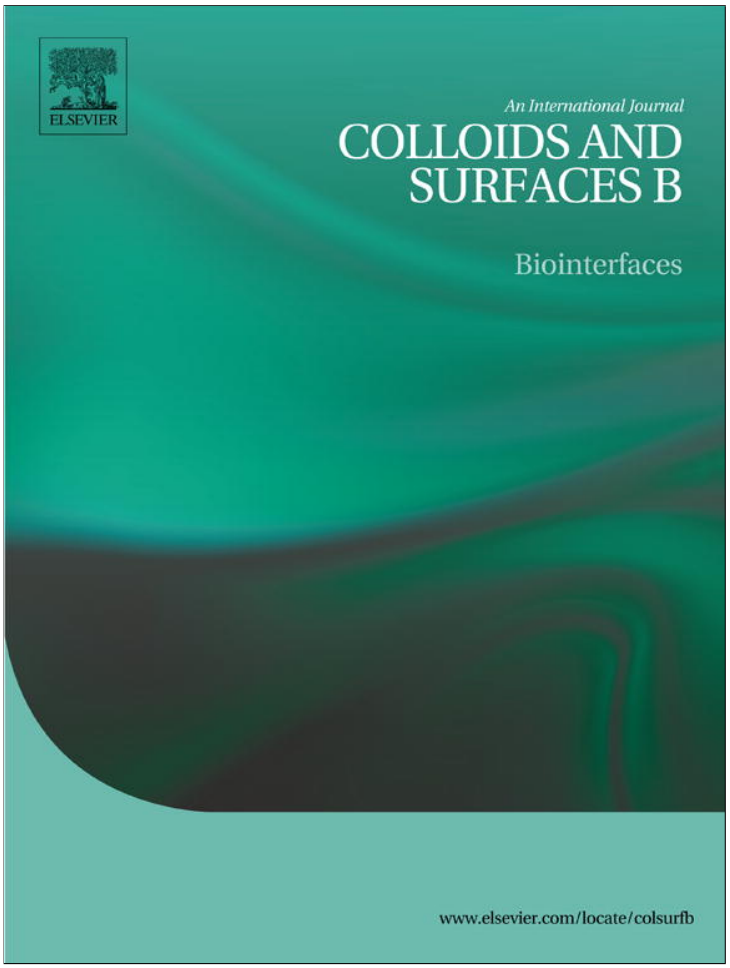

(This is a sample cover image for this issue. The actual cover is not yet available at this time.)

Colloids and Surfaces B: Biointerfaces 106 (2013) 51–59

Contents lists available at SciVerse ScienceDirect

Colloids and Surfaces B: Biointerfaces

journal homepage: www.elsevier.com/locate/colsurfb

One-step *in situ* fabrication of a granular semi-IPN hydrogel based on chitosan and gelatin for fast and efficient adsorption of Cu^{2+} ion

Wen-Bo Wang[a], Da-Jian Huang[a,b], Yu-Ru Kang[a], Ai-Qin Wang[a,*]

[a] Center for Eco-material and Green Chemistry, Lanzhou Institute of Chemical Physics, Chinese Academy of Sciences, Lanzhou 730000, PR China
[b] Graduate University of the Chinese Academy of Sciences, Beijing 100049, PR China

ARTICLE INFO

Article history:
Received 10 May 2012
Received in revised form 7 January 2013
Accepted 10 January 2013
Available online xxx

Keywords:
Chitosan
Gelatin
Granular semi-IPN hydrogel
Heavy metal
Adsorption

ABSTRACT

The novel granular semi-IPN hydrogels were *in situ* prepared in an aqueous solution by the free-radical grafting and crosslinking reactions among chitosan (CTS), acrylic acid (AA), gelatin (GE) and *N*,*N*′-methylene-*bis*-acrylamide. The FTIR spectra and elemental analysis confirmed that the AA monomers were grafted onto CTS backbone, and the GE macromolecular chains interpenetrated through the CTS-*g*-PAA network. The hydrogels are granular, which are composed of numerous micro-spheres according to the scanning electron microscope observations. The gel strength, adsorption, reuse and recovery properties of the hydrogels for Cu^{2+} ion were systematically investigated. The results indicate the hydrogel with 2 wt% GE has the highest adsorption capacity of 261.08 mg/g with the recovery ratio of 95.2%. And the incorporation of 10 wt% GE enhanced the storage modulus by 103.4% (ω = 100 rad/s) and 115.1% (ω = 0.1 rad/s), and the adsorption rate by 5.67%. Moreover, the adsorption capacity of the hydrogel is still as high as 153.9 mg/g, after five cycles of adsorption–desorption. It was found that the ion-exchange and complexation interactions between the functional groups (—COO^- and —NH_2) of the hydrogels and Cu^{2+} ion are the predominant adsorption mechanisms.

1. Introduction

Hydrogel is a moderately crosslinked functional polymer material with unique 3D network structure and large amounts of functional groups. Up to now, hydrogels have been extensively applied as water-saving materials [1–3], smart drug-delivery carriers [4–6], nano-reactor [7], and high-efficient adsorbents for removing heavy metal ions [8,9], organic pollutants [10], ammonium nitrogen [11] and dyes [12,13] from an aqueous solution. As an adsorbent, the superhydrophilic 3D network and tailored chelating groups of hydrogel (i.e. —COOH, —COO^-, —NH_2 and —OH) endow it with faster adsorption kinetics and higher adsorption capacities for the pollutants compared to other adsorbents [14,15]. Among numerous adsorbents, the hydrogels derived from polysaccharide have gained increasing attention due to its renewable, biodegradable, non-toxic and reactive characteristics [16]. However, two major problems need to be resolved to improve the properties of such materials and extend their applications. First of all, the gel strength needs to be enhanced by designing the structure of hydrogel. In addition, most of the conventional polysaccharide-based hydrogels are in bulk gel-form [17], which requires much energy in the processes of drying, smashing and granulating. Therefore, much attention should be paid to design granular hydrogels with excellent gel strength and properties.

As the "polymer alloy", semi-interpenetrating polymer network (semi-IPN) is composed of a crosslinked polymeric network and a linear polymer, and can be frequently used to improve the mechanical strength of hydrogel [18]. Gelatin (GE), an ionic hydrophilic linear polymer with the —NH_2 and —COOH functional groups, shows excellent water solubility, non-toxicity, biodegradability and compatibility. It has been proven that GE can improve the network structure and enhance the gel strength, hydrophilicity, and functional properties of hydrogels [19,20]. Chitosan (CTS), produced by deacetylation of chitin, is the world's second most abundant natural hydrophilic biomacromolecule. In addition to the renewable, biocompatible, biodegradable and non-toxic advantages of CTS [21,22], the reactive —OH and —NH_2 groups on its backbone make it easy to be modified by graft copolymerization to form hydrogels with numerous functional groups [23,24]. At acid medium, the —NH_2 groups of CTS are positively charged and can assemble with anionic acrylic acid during solution polymerization [25]. It is expected that by one-step grafting polymerization, the granular products with improved gel strength will be formed via the addition of GE. Thus, the subsequent oven-drying, smashing and granulation processes can be omitted or simplified.

Here, we designed the granular chitosan-*g*-poly(acrylic acid)/gelatin (CTS-*g*-PAA/GE) semi-IPN hydrogels by *in situ* grafting and crosslinking reactions in aqueous solution using GE as

* Corresponding author. Tel.: +86 931 4968118; fax: +86 931 8277088.
E-mail address: aqwang@licp.cas.cn (A.-Q. Wang).

0927-7765/$ – see front matter © 2013 Elsevier B.V. All rights reserved.
http://dx.doi.org/10.1016/j.colsurfb.2013.01.030

the interpenetrating component. The obtained hydrogels were well characterized by Fourier transform infrared spectra (FTIR), element analysis (EA), and scanning electronic microscope (SEM). The effect of the introduction of GE on gel strength was studied, and the adsorption properties of the hydrogels were evaluated using Cu^{2+} as the model ion. Finally, the adsorption mechanism was proposed according to the XPS and FTIR analyses.

2. Experimental

2.1. Materials

CTS (average molecular weight is 300 kDa and the deacetylation degree is 0.90) was from Golden-shell Biochemical Co, Ltd. (Zhejiang, China). AA (Chemically Pure, Shanghai Shanpu Chemical Factory, Shanghai, China) was distilled under reduced pressure before use. GE was purchased from Aladdin Reagent Co., and used as received. Ammonium persulfate (APS, analytical grade, Xi'an Chemical Reagent Factory, China) and *N*,*N*′-methylene-*bis*-acrylamide (MBA, Chemically Pure, Shanghai Chemical Reagent Corp., China) were used as received. Copper acetate monohydrate (analytical grade reagent, $Cu(CH_3COO)_2{\cdot}H_2O$) was supplied by Shanghai Reagent Corp. (Shanghai, China). Other reagents used were of analytical grade and all solutions were prepared with distilled water.

2.2. Synthesis of granular CTS-g-PAA/GE semi-IPN hydrogels

CTS powder (1 g) and GE (0.18 g for 2 wt%, 0.45 g for 5 wt%, 0.95 g for 10 wt%, 1.51 g for 15 wt% and 2.01 g for 20 wt%) were dissolved in 30 mL of the aqueous solution of AA (2.3 wt%) in a 250 mL four-neck flask equipped with a mechanical stirrer, a reflux condenser, a funnel and a nitrogen line. The solution was heated to 70 °C and purged with N_2 for 30 min to remove the dissolved oxygen. Then, 15 mL of the aqueous solution containing AA (6.5 g), crosslinker MBA (0.22 g) and initiator APS (0.15 g) was added under continuous stirring. The granular product appears after about 10 min. Finally, the reaction temperature was kept at 70 °C for 3 h to complete the polymerization. A nitrogen atmosphere was maintained throughout the reaction period.

The obtained granular product was neutralized to pH 7 using 1 mol/L NaOH solution (using 2:1 (*v*/*v*) methanol/water mixture as the solvent). The neutralized product was soaked in 250 mL of methanol for 24 h to dehydrate, and the methanol was recycled and reused. This process was repeated for four times. Finally, the dewatered product was dried at 60 °C for 2 h to a constant weight. The dry product was ground, and passed through 80–120 mesh sieve (120–180 μm). The samples were coded as CTS-*g*-PAA, Semi-IPN2, Semi-IPN5, Semi-IPN10, Semi-IPN15 and Semi-IPN20 according to the content of GE.

2.3. Determination of gel strength

The gel strength of the swollen hydrogels (the water content is 99%) was determined on a Physica MCR 301 rheometer (Germany) by a rheological method [26]. The storage modulus (G') was measured using parallel plates of 25 mm diameter at 25°, and the rheological curves of G' (Pa) versus angular frequency (ω, rad/s) were recorded. The constant deformation strain is 0.5%, and ω value was defined in the range of 0.1–100 rad/s. The reported results are the averages of three measurements.

2.4. Adsorption experiments

Batch adsorption experiments were performed by contacting 50 mg of adsorbent with 25 mL of Cu^{2+} solution in a thermostatic shaker (THZ-98 A) at 30 °C and 120 rpm to reach adsorption equilibrium. The solution was separated from the adsorbents by a 160-mesh stainless-steel sieve and the concentration of Cu^{2+} before and after the adsorption was measured by flame atomic absorption spectrometry (Z-2000, Hitachi). The adsorption capacities of the hydrogel for Cu^{2+} ion were calculated by the following equation:

$$q = (C_0 - C_e)\frac{V}{m} \quad (1)$$

where q is the adsorption amount of Cu^{2+} ion at time t (q_t, mg/g) or at equilibrium (q_e, mg/g), V is the volume of Cu^{2+} solution used (mL), C_0 and C_e are the initial and final Cu^{2+} concentration (mg/L) and m is the mass of the adsorbent used (mg). In current work, a set of Cu^{2+} solutions with the concentrations in the range of 190–1588 mg/L (pH 5.75) were used to study the adsorption isotherms. The adsorption capacities were calculated using Eq. (1). All experiments were parallel carried out for three times, and the averages were used for the analysis.

The adsorption kinetics were determined according to the following procedure: 25 mL of the Cu^{2+} solution (pH 5.75; initial concentration, 635 mg/L) was fully contacted with 50 mg of adsorbent, and then the solution was separated from the adsorbent by filtering at different time intervals (1–60 min). The amount of residual Cu^{2+} ion in the filtrate was determined, and the adsorption amounts at a given time were calculated using Eq. (1). In all cases, three parallel measurements were carried out to obtain the mean value of q and the ±SD is less than 1.5%.

2.5. Evaluation of regeneration and recovery capabilities

Typically, 70 mg of CTS-*g*-PAA, semi-IPN2 and semi-IPN10 hydrogel adsorbents were fully contacted with 25 mL of 635 mg/L Cu^{2+} solution (pH 5.75) to reach adsorption equilibrium. The Cu^{2+}-loaded adsorbents were de-adsorbed by 25 mL of 0.05 mol/L HCl solution under magnetic stirring for 60 min. The adsorbent was separated from the solution by centrifugation. The de-adsorbed adsorbent was regenerated using 0.1 mol/L NaOH solution, washed with distilled water for three times, and then dried in an oven at 70 °C for reuse. The content of Cu^{2+} in the de-adsorbed solution was determined to calculate the recovery ratio. The consecutive adsorption–desorption process was performed for five times, and the adsorption capacity and recovery ratio of the adsorbent regenerated for different times were obtained.

2.6. Characterizations

FTIR spectra were recorded on a Nicolet NEXUS FTIR spectrometer in 4000–400 cm^{-1} region using KBr pellets. Elemental analysis (C, H and N) was conducted on an Elementar Vario EL Elemental Analyzer (Elementar, Germany). SEM observation was carried out using a JSM-5600LV SEM instrument (JEOL) after coating the sample with a layer of gold film. The specific surface area (S) of the samples was determined using the BET method (Micromeritics, ASAP 2010) at 77 K. The XPS spectra were recorded on a Thermon Scientific K-Alpha-surface Analysis X-ray photoelectron spectroscope equipped with X-ray monochromatization.

3. Results and discussion

3.1. In situ preparation of granular CTS-g-PAA/GE semi-IPN hydrogels

Fig. 1 shows the proposed formation mechanism of the semi-IPN structure of the granular hydrogel. Typically, the electrostatic assembly of positively charged CTS and GE with the negatively charged AA, and the associated grafting and crosslinking reaction

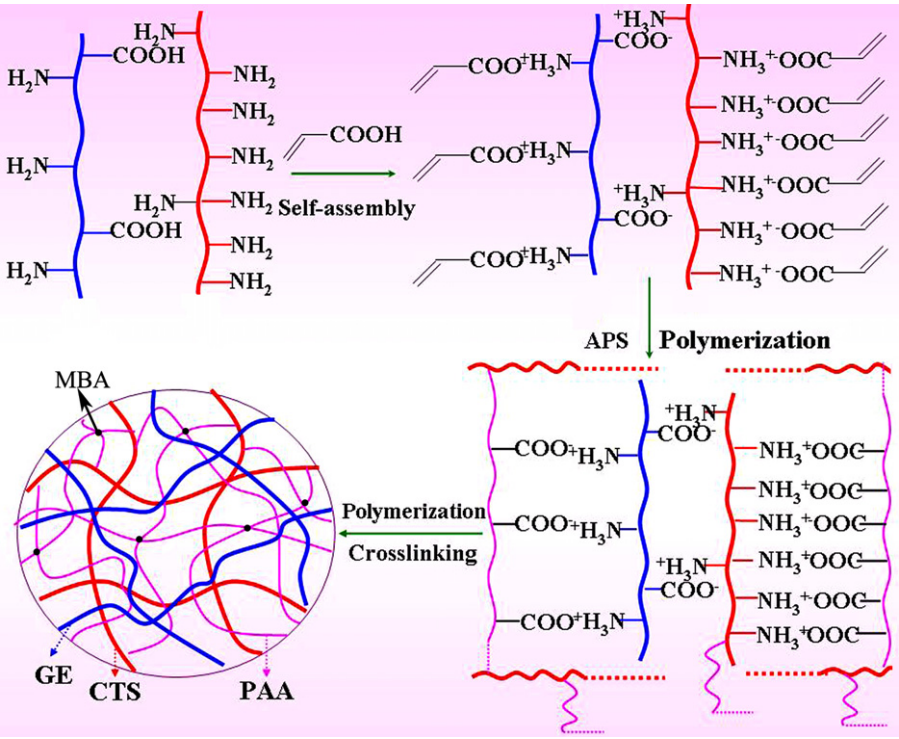

Fig. 1. Proposed formation mechanism of the granular CTS-*g*-PAA/GE semi-IPN hydrogel.

cause the formation of granular semi-IPN hydrogels. The $-NH_2$ groups of CTS and GE can be protonated by the H^+ of AA, which generated electrostatic interaction with the $-COO^-$ groups to form $-NH_3^+\cdots-OOC-$ pairs. Also, the hydrogen bonding interaction among–NH_2, —COOH and —OH groups contributes to the association of AA, CTS and GE. Upon being initiated to polymerize, the AA monomers could be grafted onto CTS backbone to form grafted poly(acrylic acid) chains, which may entangle with the CTS and GE macromolecular chains to form large amounts of insoluble particles [25,27]. In the presence of crosslinker, the grafted chains can be crosslinked to form a network structure, and these particles may aggregate with each other to form a granular product.

3.2. FTIR spectra and elemental analysis

Fig. 2 shows the FTIR spectra of CTS, GE, CTS-*g*-PAA, Semi-IPN10 and Semi-IPN20 hydrogels. As can be seen from Fig. 2(a), the characteristic absorption bands of CTS appeared at 3384 cm^{-1} (O—H stretching vibration), 1657 cm^{-1} (C=O stretching in secondary amide, amide I), 1566 cm^{-1} (N—H bending vibration of $-NH_2$ groups), 1407 cm^{-1} (C—H bending vibration of CH_2), 1154 cm^{-1} (C—O stretching of ring ether), 1069 and 1032 cm^{-1} (O—H bending vibration) [28,29]. After reacted with AA, the new bands at 1565 cm^{-1} (COO asymmetric stretching of $-COO^-$ groups), 1452 and 1408 cm^{-1} (COO symmetric stretching of $-COO^-$ groups) were observed, while the C—O(H) absorption bands of CTS at 1069 and 1032 cm^{-1} were obviously weakened (Fig. 2(c)). This indicates that AA monomers were grafted onto the CTS backbone [30]. GE shows characteristic absorption bands at 1632 cm^{-1} (amide I), 1548 cm^{-1} (C=O stretching band of $-COO^-$ groups) and 1456 cm^{-1} (COO symmetric stretching of $-COO^-$ groups) (Fig. 2(b)). With the formation of semi-IPN hydrogel, the absorption band of GE at 1632 cm^{-1} shifted to 1645 cm^{-1} (for Semi-IPN10, Fig. 2(d)) and 1648 cm^{-1} (for Semi-IPN20, Fig. 2(e)), and the intensity of bands was increased with the increase of GE content. This indicates that GE exists in the hydrogel network, and combines with the CTS-*g*-PAA network by the hydrogen bonding and electrostatic interactions among —COOH, $-NH_2$ and —OH groups to form a semi-IPN network [31].

Besides, the elemental analysis result also confirms the existence of GE in the hydrogel. The nitrogen content of CTS-*g*-PAA is 0.91 wt%, which increases to 1.08 wt% for semi-IPN2 and 1.90 wt% for semi-IPN10. This result indicates that the GE chains have formed semi-IPN structure with CTS-*g*-PAA, which is consistent with the FTIR results.

3.3. Morphology and BET analysis

Fig. 3 showed the digital photos of the semi-IPN hydrogels before dewatering, after dewatering and drying as well as the SEM micrographs of dry granules. It can be observed that the one-step polymerization of CTS, AA and GE in aqueous solution can directly form a granular product with uniform size (Fig. 3 (a)). After dewatering using methanol, the granular product becomes dense and the granular shape is retained (Fig. 3(b)). After the dewatered product was dried, the individual granular product with no aggregation was obtained (Fig. 3(c)). As shown in Fig. 3(d) and (e), numerous microspheres (or micro-particles) were observed, which connected with each other to form macro-granular congeries. This provides a direct evidence for the formation mechanism of granular product as discussed above. Among these cumulate micro-spheres, gaps and pores can be obviously observed. In order to evaluate the porosity of the product, the BET specific surface area (*S*) for the bulk gel-like CTS-*g*-PAA, the granular CTS-*g*-PAA and semi-IPN10 samples were determined. The bulk hydrogel has an *S* value of 0.013 m^2/g, whereas the *S* values reached 1.234 m^2/g for granular CTS-*g*-PAA and 2.136 m^2/g for Semi-IPN10. The improved porosity is of benefit for the penetration of external adsorbate into the hydrogel network.

3.4. Gel strength

The gel strengths of the hydrogels were determined by a rheological method, and are denoted as a function of *G′*

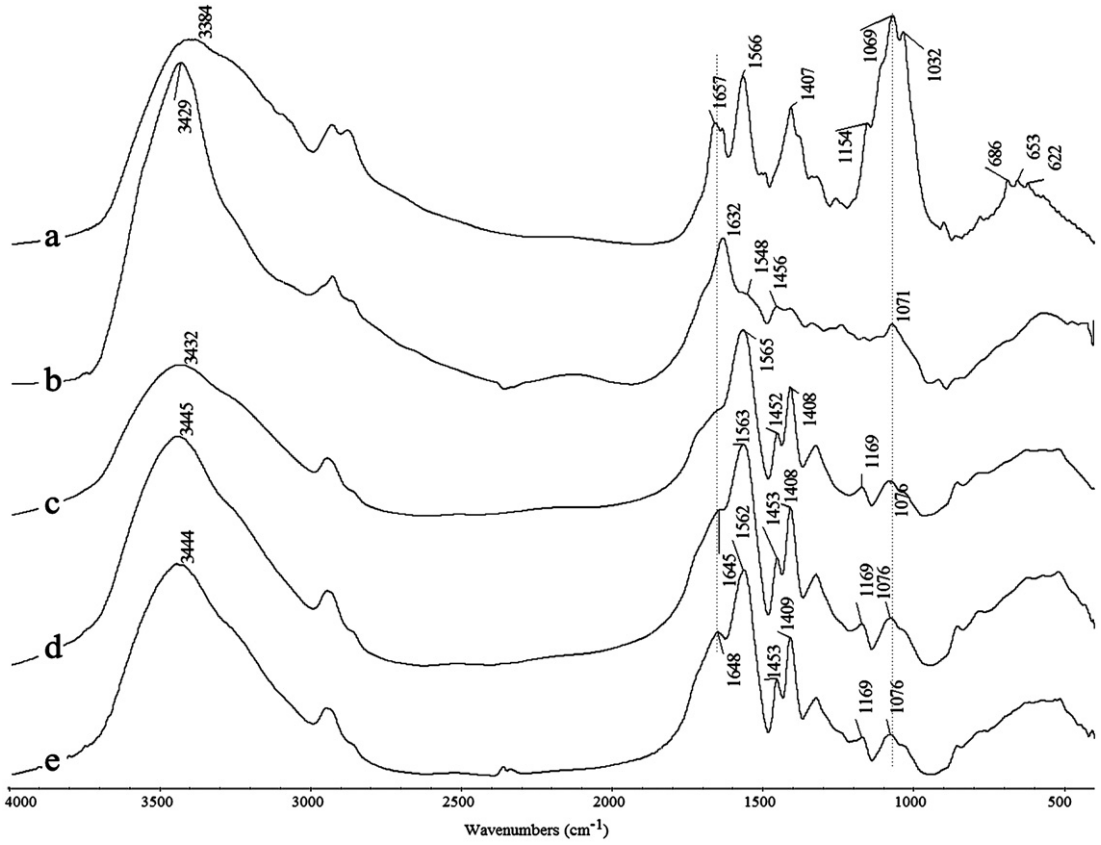

Fig. 2. FTIR spectra of (a) CTS, (b) GE, (c) CTS-*g*-PAA, (d) semi-IPN10 and (e) semi-IPN20.

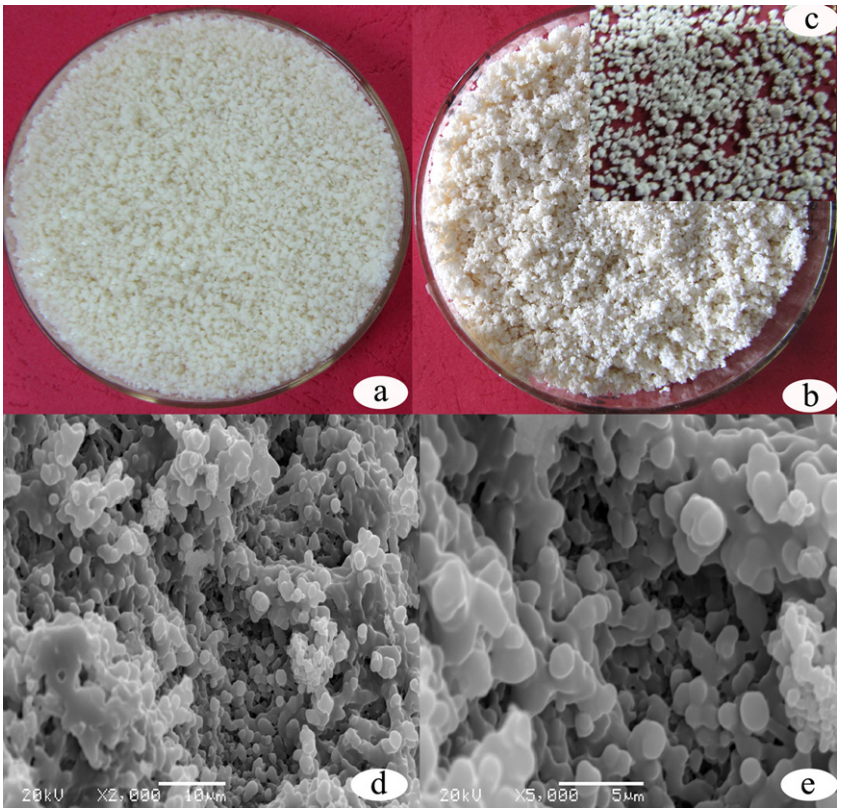

Fig. 3. The digital photos of the formed semi-IPN hydrogel before dewatering (a), after dewatering by methanol (b) and after drying (c); the SEM micrographs of the Semi-IPN10 hydrogel at magnification of 2000× (d) and 5000× (e).

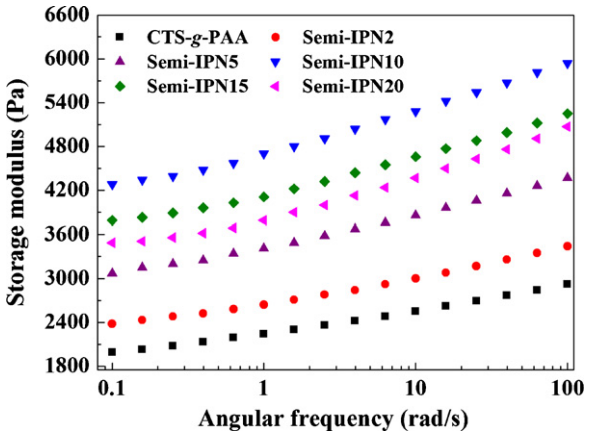

Fig. 4. Angular frequency (ω) dependence of the storage modulus (G') at a constant strain (0.5%) for the hydrogels with various amounts of GE.

(Pa) versus ω (rad/s) (Fig. 4). As shown in Fig. 4, the G' of the hydrogels clearly increased with increasing the content of GE, and reached a maximum value at 10 wt% GE (5.94 kPa, ω = 100 rad/s; 4.28 kPa, ω = 0.1 rad/s). The G' values of all semi-IPN hydrogels are higher than that of GE-free hydrogel, with the order of semi-IPN10 > semi-IPN15 > semi-IPN20 > semi-IPN5 > semi-IPN2 > CTS-*g*-PAA. This result indicates that GE makes a remarkable contribution to the elastic behavior and gel strength of the hydrogel. The significant improvement of gel strength is closely related to the change in the ingredient and structure of 3-dimensional gel network. GE contains many —COOH and —NH_2 functional groups, which can form hydrogen bonds with the —OH, —COOH and —NH_2 groups in CTS-*g*-PAA network. Thus, GE chains may entangle with the network to generate a physical crosslinking, which results in the increase of the gel strength [20]. With further increasing the GE content, the viscosity of the reactive system increased, which restricted the efficiency of chain transfer reaction and affected the formation of a stable polymer network. As a result, the storage modulus of the hydrogel decreased with the further increase of GE content.

3.5. Effect of pH on adsorption capacity

pH is an important parameter for an adsorption process because it can affect both the surface properties of adsorbent and the state of adsorbate in aqueous solution. Fig. 5 shows the effects of pH on the adsorption capacity of the hydrogels for Cu^{2+}. Clearly, the adsorption capacities of all the hydrogels for Cu^{2+} were low at pH 2. With increasing the pH, the adsorption capacity was remarkably increased and the maximum was reached at pH 5.75. This may be ascribed to the protonation of the —COO^- and —NH_2 functional groups in the 3-dimensional network at an acidic medium. The protonated groups showed relatively lower complexation with metal ions and ion-exchange capacity, and thus the adsorption capacity was decreased. However, the —COOH and —NH_3^+ groups were converted to —COONa and —NH_2 groups, which have stronger complexing and exchanging capabilities to metal ions. Thus, the adsorption capacity can be significantly increased with increasing pH. To avoid the formation of precipitation, pH 5.75 was chosen and used for the subsequent adsorption experiments.

3.6. Adsorption isotherms

As shown in Fig. 6, the adsorption capacities sharply increased with increasing the initial concentration of Cu^{2+} to 635 mg/L. Afterward, the increasing trend became flat and adsorption equilibrium was almost reached. The significant dependence of adsorption capacities on the concentration is because that the driving force at the solid–liquid interface (ion exchange, electrostatic attraction and chelation) was increased with increasing the initial ion concentration, which contributes to enhancing the adsorption and holding capacities of the hydrogel for metal ions. However, when the metal ions adsorbed by the functional groups and 3-dimensional network are close to a saturation value, the transport of ions to the adsorption sites becomes difficult. As expected, the increasing trend of the adsorption capacity becomes slower. The correlation of adsorption data with the adsorbents using a theoretical or empirical equation is essential to reveal the extent of adsorption and relevant mechanism [32], and so the Langmuir (Eq. (2)) [33] and the Freundlich (Eq. (3)) [34] isotherm models were introduced.

$$\frac{C_e}{q_e} = \frac{1}{q_m b} + \frac{C_e}{q_m} \quad (2)$$

$$\log q_e = \log K + \left(\frac{1}{n}\right) \log C_e \quad (3)$$

where q_e is the equilibrium adsorption capacities of the hydrogels for Cu^{2+} ion (mg/g); C_e is the concentration of Cu^{2+} ions after adsorption (mg/L); q_m is the maximum adsorption capacity (mg/g); b is the Langmuir adsorption constant (L/mg), which is related to the free energy of adsorption. K (L/g) and n (dimensionless) are

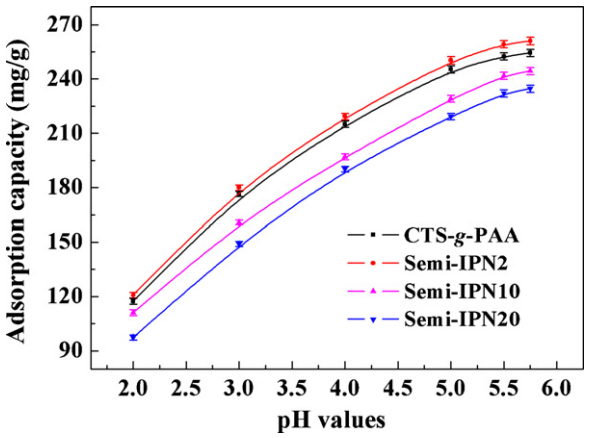

Fig. 5. Effects of pH on the Cu^{2+} adsorption (initial Cu^{2+} concentration, 635 mg/L; adsorption time, 60 min; adsorbent dosage, 2 g/L). The error bars denote the standard deviation (SD < 1.5%, n = 3).

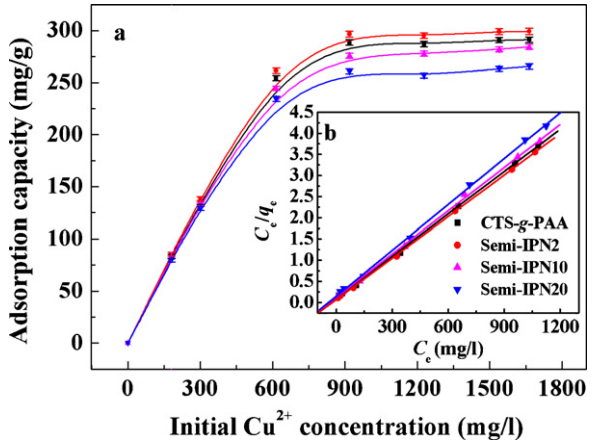

Fig. 6. (a) Effect of initial Cu^{2+} concentrations on the adsorption capacity, and (b) the plots of C_e/q_e versus C_e for Langmuir isotherm model. The initial pH, 5.75; adsorbent dosage, 2 g/L. The error bars denote the standard deviation (SD < 1.5%, n = 3).

Table 1
Estimated adsorption isotherm parameters for the adsorption of Cu^{2+} ion onto the hydrogels.

Samples	Langmuir equation			Freundlich equation		
	q_m (mg/g)	b (L/mg)	R^2	K	n	R^2
CTS-*g*-PAA	300.31	0.0356	0.9998	52.36	3.7543	0.9195
Semi-IPN2	305.82	0.0486	0.9999	61.65	4.0514	0.9259
Semi-IPN10	294.13	0.0271	0.9997	48.19	3.6784	0.9275
Semi-IPN20	277.04	0.0244	0.9996	43.36	3.6129	0.9246

the Freundlich isotherm constant and the heterogeneity factor, respectively. These parameters can be obtained by fitting experimental data to the Langmuir (C_e/q_e versus C_e) and Freundlich ($\log q_e$ versus $\log C_e$) isotherm models (Table 1). As can be seen, the data fitted by Freundlich isotherm model ($R^2 < 0.9447$) have great difference with the experimental values, whereas the data fitted by the Langmuir isotherm model ($R^2 > 0.9997$) is almost equal to the experimental value. This means the Langmuir model is suitable for evaluating the adsorption isotherm. As is well known, the Langmuir model is based on the assumption of a structurally homogeneous adsorbent where all adsorption sites are identical and energetically equivalent, and the Freundlich isotherm model describes reversible adsorption and is not restricted to the formation of monolayer. From the above results, it can be concluded that a monolayer of Cu^{2+} ions was formed on the surface of the hydrogels. In addition, it can be clearly observed from Table 2 that the granular semi-IPN hydrogel adsorbents show higher adsorption capacity than the raw chitosan powder and the other adsorbents reported.

3.7. Adsorption kinetics

Adsorption rate is especially important for the practical application of an adsorbent. As shown in Fig. 7, the adsorption amount of each hydrogel for Cu^{2+} ion shows a rapid increase with prolonging the contact time (t, s), and the adsorption equilibrium can be almost reached within 10 min. For exploring the adsorption mechanism, such as mass transfer and chemical reaction, the pseudo-first-order and pseudo-second-order kinetic equations were used to express the adsorption data [41]:

$$\log(q_e - q_t) = \log q_e - \left(\frac{k_1}{2.303}\right) t \quad (4)$$

$$\frac{t}{q_t} = \frac{1}{k_2 q_e^2} + \frac{t}{q_e} \quad (5)$$

where q_e and q_t are the adsorption capacities of the hydrogels for Cu^{2+} ion (mg/g) at equilibrium and time t (s), respectively. k_1 is the rate constant of pseudo-first-order (s^{-1}), and k_2 is the rate constant of pseudo-second-order adsorption kinetic (mg/(g s)). k_1 and k_2 values can be calculated by the slope and intercept from the straight lines of $\log(q_e - q_t)$ against t and t/q_t versus t, respec-

Table 2
Comparison of the adsorption capacities of different adsorbents for Cu^{2+} ion.

Adsorbents	q_m (mg/g)	Ref.
Polymer modified pine bark	45.05	[35]
Tamarindus indica seed powder	133.24	[36]
Magnetic chitosan microspheres	66.70	[37]
Tetraethylenepentamine-modified poly(glycidyl methacrylate-co-trimethylolpropane trimethacrylate) microspheres	64.77	[38]
Magnetic Cu(II) ion imprinted composite	71.36	[39]
Starch-g-poly(acrylic acid)/sodium humate Hydrogel	179.84	[40]
Raw chitosan powder	84.21	This work
Semi-IPN2	305.82	This work
Semi-IPN10	294.13	This work

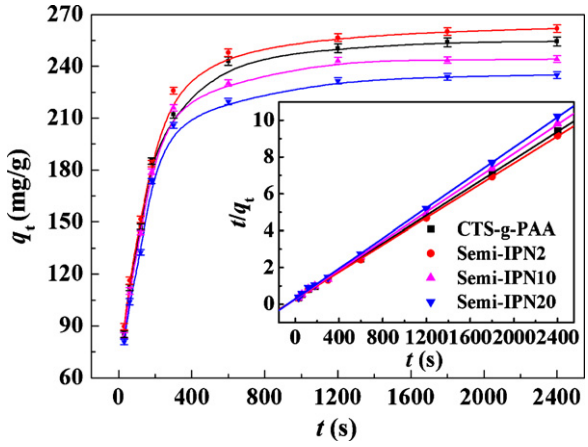

Fig. 7. (a) Influences of contact time on the adsorption capacities; (b) the plots of t/q_t versus t. The initial Cu^{2+} concentration, 635 mg/L; initial pH, 5.75; adsorbent dosage, 2 g/L. The error bars denote the standard deviation (SD < 1.5%, $n = 3$).

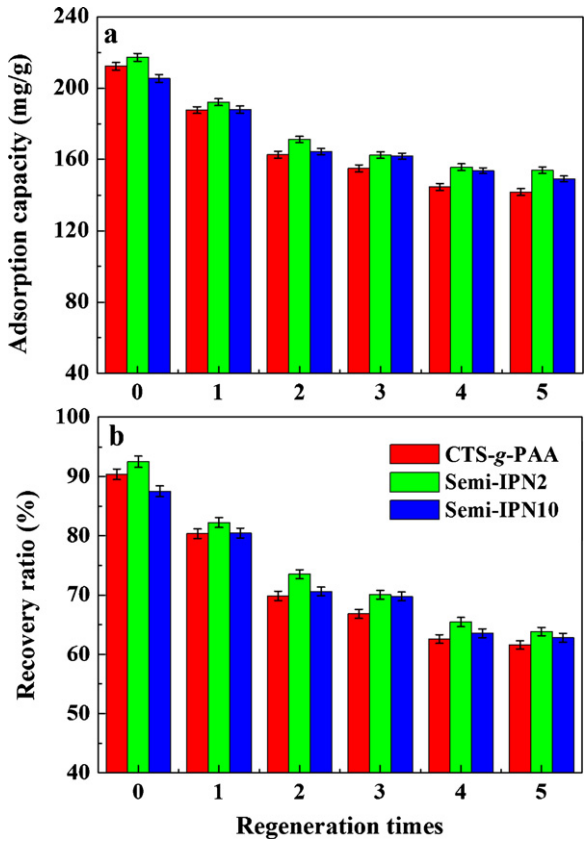

Fig. 8. Regeneration (a) and recovery (b) capabilities of the hydrogels for Cu^{2+} ions. The error bars denote the standard deviation (SD < 1.5%, $n = 3$).

Table 3
Estimated adsorption kinetic parameters for Cu^{2+} adsorption.

	Pseudo-first-order model				Pseudo-second-order model			
	$q_{e,exp}$ (mg/g)	$q_{e,cal}$ (mg/g)	k_1 (s^{-1})	R^2	$q_{e,cal}$ (mg/g)	$k_2 \times 10^5$ (g/(mg s))	k_{2i} (mg/(g s))	R^2
CTS-*g*-PAA	254.42	137.62	0.00316	0.9887	261.12	5.3305	3.6345	0.9999
Semi-IPN2	261.08	124.31	0.00256	0.9724	268.31	5.1899	3.7362	0.9999
Semi-IPN10	244.44	122.46	0.00332	0.9748	250.53	6.1185	3.8403	0.9998
Semi-IPN20	234.63	115.94	0.00281	0.9827	240.74	5.9080	3.4240	0.9999

tively (Table 3). The initial adsorption rate constant k_{2i} (mg/(g s)) can be determined using the relation of $k_{2i} = k_2 q_e^2$ according to the pseudo-second-order adsorption kinetics (Table 3). It can be seen from Table 3 that the fitting results of pseudo-first-order kinetic equation do not give the theoretical q_e values that agree well with the experimental values, whereas the linear correlation coefficient (R^2) of the pseudo-second-order kinetic plots for the adsorption of the hydrogel for Cu^{2+} ion is above 0.999. This indicates that the pseudo-second-order kinetic model is suitable for fitting the adsorption kinetics and the adsorption process of Cu^{2+} ion onto the semi-IPN hydrogel is probably controlled by the chemical process. From Table 3, it is obvious that the initial adsorption rate of the hydrogel for Cu^{2+} ion is in the order of Semi-IPN10 > Semi-IPN2 > CTS-*g*-PAA > Semi-IPN20. So, the semi-IPN hydrogel adsorbents have higher initial adsorption rate and higher adsorption capacity, and are promising adsorbents for Cu^{2+} ion.

3.8. Regeneration and recovery capabilities

The adsorbent with better regeneration capacity and recovery capacity for metal ions are desirable from the viewpoint of usage cost and recovery of valuable metals. As shown in Fig. 8, the adsorption capacity slightly decreased with increasing the

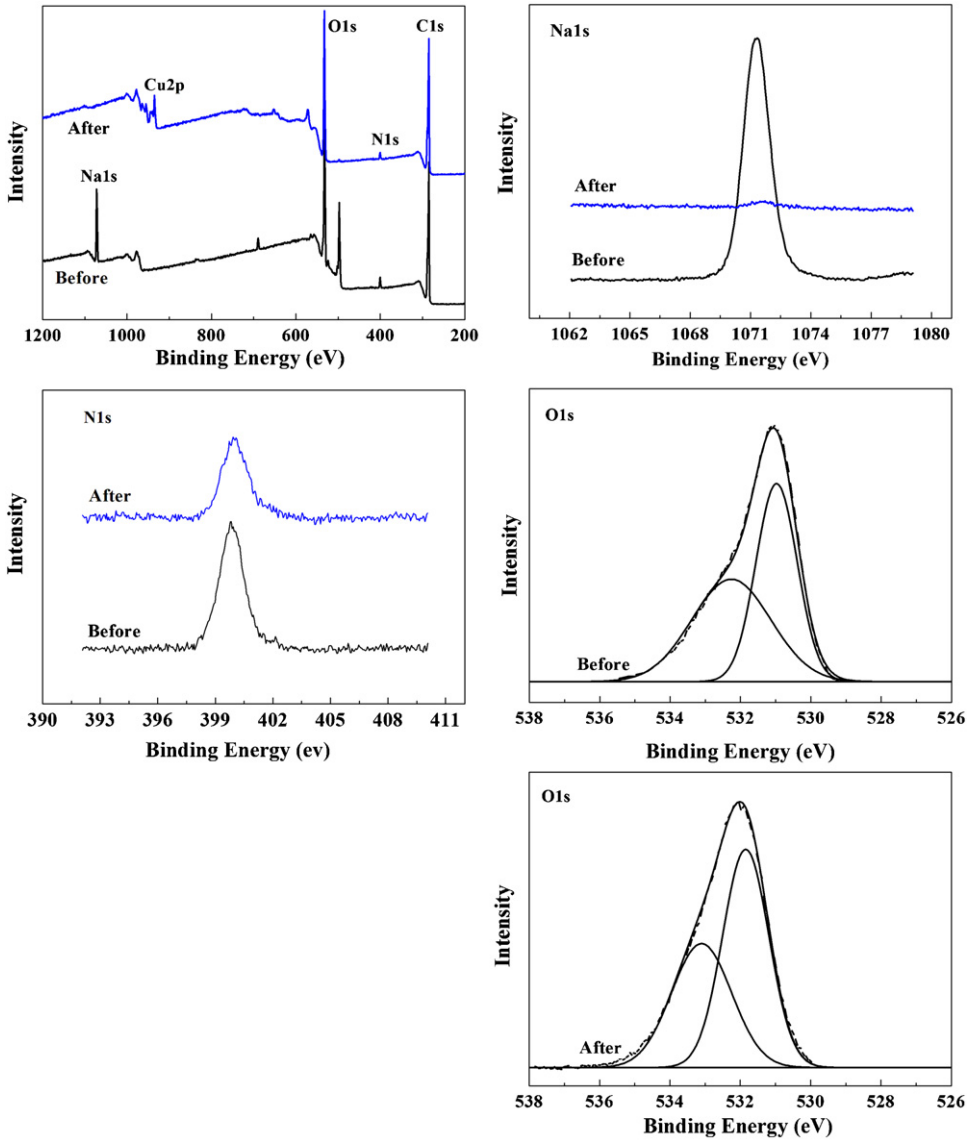

Fig. 9. XPS spectra, Na1s, N1s and O1s spectra of the hydrogel before and after Cu^{2+} adsorption.

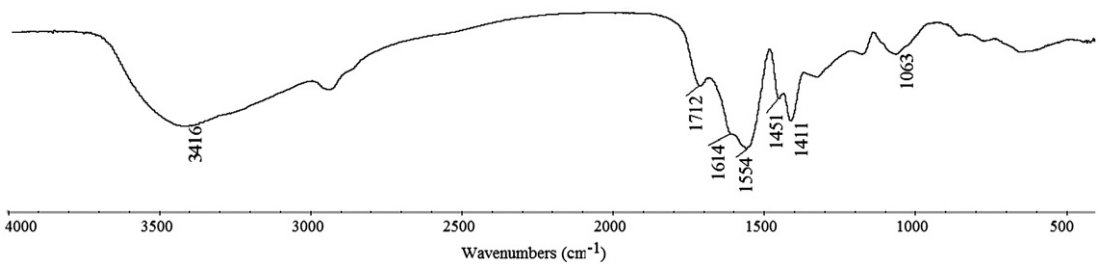

Fig. 10. FTIR spectra of the semi-IPN10 hydrogel after Cu^{2+} adsorption.

adsorption–desorption cycles, whereas the adsorption capacities are still as high as 141.8 mg/g (for CTS-*g*-PAA), 153.9 mg/g (for Semi-IPN2) and 149.2 mg/g (for Semi-IPN10) after regeneration for five times. The adsorbed Cu^{2+} ions can be rapidly and easily de-absorbed by diluted HCl solution to transform as the soluble and reutilized $CuCl_2$ salts. As can be seen from Fig. 8b, the recovery ratio of Cu^{2+} ion from the initial solution (635 mg/L; pH 5.75; 25 mL) reached 90.4% (CTS-*g*-PAA), 92.5% (Semi-IPN2) and 87.5% (Semi-IPN10) for the first cycle, and 61.6% (CTS-*g*-PAA), 63.9% (Semi-IPN2) and 62.8% (Semi-IPN10) for the fifth regeneration, respectively. This indicates that the granular hydrogels have better recovery capacity for Cu^{2+} ions, and the presence of GE improves its regeneration and recovery capabilities.

3.9. Adsorption mechanism

XPS spectra were frequently used to distinguish the different forms of the same element and to identify the existence of a particular element in a material, and can be used to explore the adsorption mechanism [42]. Fig. 9 shows the XPS spectra of the semi-IPN hydrogel before and after the adsorption. It is obvious that the Cu2p (binding energy = 933.53 eV) peak appeared in the spectra of the hydrogel after the adsorption, indicating that the Cu^{2+} ions were adsorbed on the hydrogel. The typical Na1s peak of the hydrogel with the bonding energy of 1071.33 eV almost disappeared after the adsorption, indicating that the Na^+ ion was exchanged with the Cu^{2+} ions during the adsorption process. The N1s exhibited a single peak with the bonding energy of 399.83 eV (the N atom in the R—NH_2 group), and slightly shifted to 399.99 eV after the adsorption, confirming that the nitrogen atom of —NH_2 groups could also form surface complexes with Cu^{2+} ions [43]. The O1s peaks at 530.97 eV (C=O) and 532.26 eV (C—O) for the hydrogel shifted to 531.85 (C=O) and 533.10 (C—O), respectively after Cu^{2+} adsorption. This indicates that the —COO^- groups complexed with the metal ions, and a chemical adsorption process occurred [44]. In order to further illustrate the adsorption mechanism of the hydrogel for Cu^{2+} ions, the FTIR spectrum of the hydrogel after adsorption was recorded (Fig. 10). Compared with the spectrum of the semi-IPN hydrogel before adsorption, the asymmetric stretching vibration of —COO^- groups at 1563 cm^{-1} was shifted to 1554 cm^{-1} after adsorbing Cu^{2+}, indicating that the —COO^- groups complexed with the metal ions [40].

4. Conclusions

The granular CTS-*g*-PAA/GE semi-IPN hydrogels were in situ synthesized in an aqueous solution through one-step grafting polymerization and crosslinking reaction of CTS, GE and AA. The formation of —$NH_3^+ \cdots$—OOC— electrostatic pairs and hydrogen bonding interactions among CTS, GE and AA induced the generation of granular product. The hydrogel with a coarse surface are composed of many micro-spheres stacked with each other. By forming the semi-IPN structure, the linear GE enhanced the gel strength by 115.1% (ω = 0.1 rad/s) with 10 wt% GE. The optimal semi-IPN hydrogel shows higher adsorption capacity (261.08 mg/g) and adsorption rate for Cu^{2+} ions. The adsorption kinetics was satisfactorily fitted by pseudo-second-order kinetic model due to the chemical adsorption resulting from the functional groups. After regeneration for 5 times, the adsorption capacities are still as high as 141.8 mg/g (for CTS-*g*-PAA), 153.9 mg/g (for Semi-IPN2) and 149.2 mg/g (for Semi-IPN10), and the respective recovery ratio reached 61.6%, 63.9% and 62.8%. FTIR and XPS analysis revealed that the chemical complexation of —COO^- and —NH_2 functional groups and ion-exchange are the main adsorption mechanisms. In addition, this work can be taken as a part of efforts to reduce the excessive consumption of petroleum-based polymers and to develop a new type of biopolymer-based adsorbents.

Acknowledgement

This work is supported by the National Natural Science Foundation of China (Nos. 51003112 and 21107116).

References

[1] M. Teodorescu, A. Lungu, P.O. Stanescu, C. Neamţu, Preparation and properties of novel slow-release NPK agrochemical formulations based on poly (acrylic acid) hydrogels and liquid fertilizers, Ind. Eng. Chem. Res. 48 (2009) 6527.
[2] C. Nakason, T. Wohmang, A. Kaesaman, S. Kiatkamjornwong, Preparation of cassava starch-graft-polyacrylamide superabsorbents and associated composites by reactive blending, Carbohydr. Polym. 81 (2010) 348.
[3] Y. Chen, Y.F. Liu, H.M. Tan, J.X. Jiang, Synthesis and characterization of a novel superabsorbent polymer of *N*,*O*-carboxymethyl chitosan graft copolymerized with vinyl monomers, Carbohydr. Polym. 75 (2009) 287.
[4] C. Silan, A. Akcali, M.T. Otkun, N. Ozbey, S. Butun, O. Ozay, N. Sahiner, Novel hydrogel particles and their IPN films as drug delivery systems with antibacterial properties, Colloids Surf. B: Biointerfaces 89 (2012) 248.
[5] N. Bhattarai, J. Gunn, M.Q. Zhang, Chitosan-based hydrogels for controlled, localized drug delivery, Adv. Drug Deliv. Rev. 62 (2010) 83.
[6] S.S. Vaghania, M.M. Patelb, C.S. Satishc, Synthesis and characterization of pH-sensitive hydrogel composed of carboxymethyl chitosan for colon targeted delivery of ornidazole, Carbohydr. Res. 347 (2012) 76.
[7] H. Saeidian, F.M. Moghaddam, A. Pourjavadi, S. Barzegar, R. Soleymana, A. Sohrabib, Superabsorbent polymer as nanoreactors for preparation of hematite nanoparticles and application of the prepared nanocatalyst for the Friedel–Crafts acylation, J. Braz. Chem. Soc. 20 (2009) 466.
[8] I. Kavianinia, P.G. Plieger, N.G. Kandile, D.R.K. Harding, New hydrogels based on symmetrical aromatic anhydrides: synthesis, characterization and metal ion adsorption evaluation, Carbohydr. Polym. 87 (2012) 881.
[9] M.R. Guilherme, A.V. Reis, T.A. Paulino, T.A. Moia, L.H.C. Mattoso, E.B. Tambourgi, Pectin-based polymer hydrogel as a carrier for release of agricultural nutrients and removal of heavy metals from wastewater, J. Appl. Polym. Sci. 117 (2010) 3146.
[10] P. Rao, I.M.C. Lo, K. Yin, S.C.N. Tang, Removal of natural organic matter by cationic hydrogel with magnetic properties, J. Environ. Manage. 92 (2011) 1690.
[11] Y.A. Zheng, A.Q. Wang, Preparation, ammonium adsorption property of biotite-based hydrogel composite, Ind. Eng. Chem. Res. 49 (2010) 6034.
[12] J.Y. Wang, H.M. Wang, Z.J. Song, D.L. Kong, X.M. Chen, Z.M. Yang, A hybrid hydrogel for efficient removal of methyl violet from aqueous solutions, Colloids Surf. B: Biointerfaces 80 (2010) 155.
[13] B. Özkahraman, I. Acar, S. Emik, Removal of cationic dyes from aqueous solutions with poly (N-isopropylacrylamide-co-itaconic acid) hydrogels, Polym. Bull. 66 (2011) 551.
[14] Y. Liu, W.B. Wang, A.Q. Wang, Adsorption of lead ions from aqueous solution by using carboxymethylcellulose-g-poly (acrylic acid)/attapulgite hydrogel composites, Desalination 259 (2010) 258.

[15] E.K. Yetimoğlu, M.V. Kahraman, Ö. Ercan, N-vinylpyrrolidone/acrylic acid/2-acrylamido-2-methylpropane sulfonic acid based hydrogels: Synthesis, characterization and their application in the removal of heavy metals, React. Funct. Polym. 67 (2007) 451.
[16] W.S. Wan Ngah, L.C. Teong, M.A.K.M. Hanafiah, Adsorption of dyes and heavy metal ions by chitosan composites: a review, Carbohydr. Polym. 83 (2011) 1446.
[17] M.R. Guilherme, A.V. Reis, A.T. Paulino, A.R. Fajardo, E.C. Muniz, E.B. Tambourgi, Superabsorbent hydrogel based on modified polysaccharide for removal of Pb^{2+} and Cu^{2+} from water with excellent performance, J. Appl. Polym. Sci. 105 (2007) 2903.
[18] D. Myung, D. Waters, M. Wiseman, P. Duhamel, J. Noolandi, C.N. Ta, C.W. Frank, Progress in the development of interpenetrating polymer network hydrogels, Polym. Adv. Technol. 19 (2008) 647.
[19] M. Eid, M.A. Abdel-Ghaffar, A.M. Dessouki, Effect of maleic acid content on the thermal stability, swelling behaviour and network structure of gelatin-based hydrogels prepared by gamma irradiation, Nucl. Instrum. Methods Phys. Res. B 267 (2009) 91.
[20] A. Nakayama, A. Kakugo, J.P. Gong, Y. Osada, M. Takai, T. Erata, S. Kawano, High mechanical strength double-network hydrogel with bacterial cellulose, Adv. Funct. Mater. 14 (2004) 1124.
[21] S. Sundar, J. Kundu, S.C. Kundu, Biopolymeric nanoparticles, Sci. Technol. Adv. Mater. 11 (2010) 014104.
[22] S.S. Vaghani, M.M. Patel, Protein micro and nanoencapsulation within glycol-chitosan/Ca^{2+}/alginate matrix by spray drying, Curr. Drug Discov. Technol. 8 (2011) 126.
[23] H.H. Sokker, A.M. Abdel Ghaffar, Y.H. Gad, A.S. Aly, Synthesis and characterization of hydrogels based on grafted chitosan for the controlled drug release, Carbohydr. Polym. 75 (2009) 222.
[24] J.H. Choi, S. Lee, H.J. Kang, J.Y. Lee, J. Kim, H.O. Yoo, T.R. Stratton, B.M. Applegate, J.P. Youngblood, H.J. Kim, K.N. Ryu, Synthesis of water-soluble chitosan-g-PEO and its application for preparation of superparamagnetic iron oxide nanoparticles in aqueous media, Macromol. Res. 18 (2010) 504.
[25] Y. Hua, X.Q. Jiang, Y. Ding, H.X. Ge, Y.Y. Yuan, C.Z. Yang, Synthesis and characterization of chitosan-poly(acrylic acid) nanoparticles, Biomaterials 23 (2002) 3193.
[26] M.J. Ramazani-Harandi, M.J. Zohuriaan-Mehr, A.A. Yousefi, A. Ershad-Langroudi, K. Kabiri, Rheological determination of the swollen gel strength of superabsorbent polymer hydrogels, Polym. Test. 25 (2006) 470.
[27] J.W. Wang, Y.M.J. Kuo, Preparation and adsorption properties of chitosan-poly(acrylic acid) nanoparticles for the removal of nickel ions, J. Appl. Polym. Sci. 107 (2008) 2333.
[28] M.R. Kasaai, A review of several reported procedures to determine the degree of N-acetylation for chitin and chitosan using infrared spectroscopy, Carbohydr. Polym. 71 (2008) 497.
[29] S. Benamer, M. Mahlous, D. Tahtat, A. Nacer-Khodja, M. Arabi, H. Lounici, N. Mameri, Radiation synthesis of chitosan beads grafted with acrylic acid for metal ions sorption, Radiat. Phys. Chem. 80 (2011) 1391.
[30] J. Tripathy, D.K. Mishra, M. Yadav, K. Behari, Synthesis, characterization and applications of graft copolymer (Chitosan-g-N,N-dimethylacrylamide), Carbohydr. Polym. 79 (2010) 40.
[31] V. Koul, R. Mohamed, D. Kuckling, H.J.P. Adler, V. Choudhary, Interpenetrating polymer network (IPN) nanogels based on gelatin and poly(acrylic acid) by inverse miniemulsion technique: synthesis and characterization, Colloids surf. B: Biointerfaces 83 (2011) 204.
[32] E.L. Grabowska, G. Gryglewicz, Adsorption characteristics of congo red on coal-based mesoporous activated carbon, Dyes Pigm. 74 (2007) 34.
[33] I. Langmuir, The adsorption of gases on plane surfaces of glass, mica and platinum, J. Am. Chem. Soc. 40 (1918) 1361.
[34] H.M.F. Freundlich, Über die adsorption in lösungen, Z. Phys. Chem. 57 (1906) 385.
[35] M.E. Argun, S. Dursun, M. Karatas, Removal of Cd(II) Pb(II), Cu(II) and Ni(II) from water using modified pine bark, Desalination 249 (2009) 519.
[36] S. Chowdhury, P.D. Saha, Biosorption kinetics, thermodynamics and isosteric heat of sorption of Cu(II) onto *Tamarindus indica* seed powder, Colloids Surf. B: Biointerfaces 88 (2011) 697.
[37] L.M. Zhou, Y.P. Wang, Z.R. Liu, Q.W. Huang, Characteristics of equilibrium, kinetics studies for adsorption of Hg(II), Cu(II), and Ni(II) ions by thiourea-modified magnetic chitosan microspheres, J. Hazard. Mater. 161 (2009) 995.
[38] Z.Y. Yu, R.A. Wu, M.H. Wu, L. Zhao, R.B. Li, H.F. Zou, Preparation of polyamine-functionalized copper specific adsorbents for selective adsorption of copper, Colloids Surf. B: Biointerfaces 78 (2010) 222.
[39] Y.M. Ren, M.L. Zhang, D. Zhao, Synthesis and properties of magnetic Cu(II) ion imprinted composite adsorbent for selective removal of copper, Desalination 228 (2008) 135.
[40] Y.A. Zheng, S.B. Hua, A.Q. Wang, Adsorption behavior of Cu^{2+} from aqueous solutions onto starch-*g*-poly (acrylic acid)/sodium humate hydrogels, Desalination 263 (2010) 170.
[41] W. Rudzinsk, W. Plazinski, Kinetics of solute adsorption at solid/solution interfaces: a theoretical development of the empirical pseudo-first and pseudo-second order kinetic rate equations, based on applying the statistical rate theory of interfacial transport, J. Phys. Chem. B 110 (2006) 16514.
[42] L. Jin, R.B. Bai, Mechanisms of lead adsorption on chitosan/PVA hydrogel beads, Langmuir 18 (2002) 9765.
[43] D. Zhou, L.N. Zhang, S.L. Guo, Mechanisms of lead biosorption on cellulose/chitin beads, Water Res. 39 (2005) 3755.
[44] S.F. Lim, Y.M. Zheng, S.W. Zou, J.P. Chen, Characterization of copper adsorption onto an alginate encapsulated magnetic sorbent by a combined FT-IR, XPS, and mathematical modeling study, Environ. Sci. Technol. 42 (2008) 2551.